Wetting and drying of aqueous droplets containing non-ionic surfactants C_nE_m

*Jing Shi, Lisong Yang, and Colin D. Bain**

Department of Chemistry, Durham University, Durham, DH1 3LE, U.K.

KEYWORDS: Surfactants C_nE_m, sessile droplet, phase transition and separation, surfactant mesophase, Marangoni flows

ABSTRACT: This paper presents a systematic study of the wetting and drying of aqueous pico-litre droplets containing non-ionic surfactants polyoxyethylene alkyl ethers (C_nE_m; n = 10, 12, 14, m = 6 or 8) in comparison with the anionic surfactant sodium dodecyl sulfate (SDS). The spreading and drying of droplets on hydrophilic substrates were studied by tracking the three-phase contact line (TCL) and by interferometry. C_nE_m droplets undergo phase separation during drying: a water-rich droplet retracts and leaves behind a thin film that is postulated to be a surfactant mesophase. This thin film either retracts or breaks up into small droplets on a longer time scale. The receding contact angle of the water-rich droplet on the thin film in the late stage of drying of C_nE_m droplets is independent of hydrophobicity of substrates, supporting the inference that a mesophase is present on the surface. Both C_nE_m and SDS solutions inhibit spreading on hydrophilic surfaces, which is attributed to Marangoni contraction as a result of a surface tension gradient across the gas–liquid interface. More pronounced suppression of spreading is observed in the case of C_nE_m solutions, possibly due to the phase transition of surfactant solution in the vicinity of the initial

TCL leading to a viscous phase at the TCL that pins the droplet. Tracer particle measurements reveal that mild Marangoni flows exist for droplets with surfactant concentrations well above the critical micelle concentration (CMC). Origins of the surfactant gradients that result in Marangoni flows are discussed.

INTRODUCTION

Surfactants are versatile additives to improve wettability, stabilise dispersions and emulsions, fix dyes and form foams. The understanding of wetting and drying dynamics of surfactant-laden droplets on a solid surface is of great importance in industrial applications such as inkjet printing,[1-5] spray coating[6-7] and agricultural spraying.[8-10] Influences of surfactants on behaviours of sessile droplets are diverse depending on the characteristics of both surfactants and substrates. For example, the decrease in the surface tension caused by surfactants typically results in a lower contact angle and enhanced droplet spreading.[11-13] As a sessile droplet dries, the local surfactant concentration varies, being maximal close to the three-phase contact line (TCL).[14-15] The non-uniform distribution of surfactants can lead to a surface tension gradient which may induce Marangoni flows.[16-19] Furthermore, surfactants may adsorb to the solid substrate and affect substrate wettability.[20] In colloidal solutions, surfactants may adsorb to solid particles and/or substrates and further affect the particle−particle, particle−free interface and particle−substrate interactions.[21-22] Surfactants are normally involatile so as an aqueous droplet dries the surfactant concentration increases continuously, leading to phase transitions and/or phase separation that further complicate the drying process.[23-24]

A number of authors have studied the effect of specific surfactants on the morphology of deposits and/or the internal flows in drying droplets. Many of these studies were stimulated by the desire to suppress the coffee-ring-effect (CRE), in which convective flows carry suspended particles towards the TCL when droplets dry with a pinned contact line[14]. Early studies by Deegan explored the effect of SDS on particle deposition in microliter droplets.[25] Kajiya *et al.* found that the addition of a small amount of a fluorosurfactant suppressed the coffee-ring effect (CRE) in picoliter droplets of a polymer solution, which they ascribed to surfactant-induced Marangoni flows.[17] Still *et al.*

studied the evaporation of colloidal microliter drops with SDS and reported tree-ring deposition structures and relatively uniform deposition inside the inner ring at surfactant concentrations above the critical micelle concentration (CMC).[18] The authors attributed the suppression of the CRE to the observed Marangoni eddies close to the TCL, but the causes behind the Marangoni flows at surfactant concentrations above CMC were left as an open question. Anyfantakis *et al*. investigated the effect of ionic surfactants, including hexadecyltrimethylammonium bromide (CTAB), dodecyltrimethylammonium bromide (DTAB), sodium dodecylbenzenesulfonate (SDBS) and SDS, on the deposits of colloidal microliter drops at initial concentrations lower than CMC. Surfactant-mediated interactions between particles and the liquid−gas and liquid−solid interfaces were shown to define the primary morphology of deposits.[22] Kim *et al.* demonstrated the formation of uniform deposits upon the evaporation of microliter drops of a solution consisting of ethanol, water, SDS and surface-adsorbed polymer and attributed the uniformity to continuous mixing by Marangoni flows set by solute and surfactant simultaneously as well as a strong interaction between particles and substrate.[19] Marin *et al.* used astigmatism particle tracking velocimetry (APTV) to visualise three-dimensional internal flows in evaporating drops containing SDS or polysorbate 80.[26] They found that polysorbate 80 significantly reduced internal and surface flows, which they ascribed to a surfactant-induced increase of surface rigidity. More recently, Kwieciński *et al*. examined the contact-angle evolution during the evaporation of SDS-laden droplets on hydrophobic substrates. The authors observed a minimum in the contact angle during evaporation which they attributed to contact line pinning by surfactant aggregates on the substrate below the droplet.[20]

Thus far, the majority of evaporation studies have focussed on ionic surfactants such as SDS, CTAB and DTAB in microliter sessile droplets. The polyoxyethylene alkyl ethers (C_nE_m) are a class of biodegradable non-ionic surfactant that is widely used as an emulsifying agent and detergent. There are extensive studies on the thermodynamic properties of aqueous bulk solutions,[27-30] the characterisation of adsorbed layers on solid surfaces and adsorption kinetics,[31-32] the wetting dynamics of microlitre droplets[33-34] and the rheology of C_nE_m liquid crystals.[35-36] Yet, the drying characteristics of C_nE_m-laden sessile droplets remain scarcely explored. This study aimed to investigate the influence of $\mathrm{C_nE_m}$ on the wetting and drying of picolitre droplets. We systematically studied a series of polyoxyethylene surfactants, including $\mathrm{C_{10}E_8}$, $\mathrm{C_{12}E_8}$, $\mathrm{C_{14}E_8}$ and $\mathrm{C_{14}E_6}$, and compared the results with those from SDS-laden droplets. As the non-ionic surfactants have low CMCs, the initial surfactant concentrations were well above the CMC for most of our experiments. In all cases, the surfactant concentrations are above the CMC during the later stages of drying.

The droplets have a typical volume of 200±50 pL and diameters D=200 ± 50 µm after spreading on hydrophilic glass cover-slips. The typical drying time for the water-rich phase (see later) is 1 s at ambient humidity. Since concentrations are generally well above the CMC, micellar transport is more important than monomer transport. The Péclet number of micelles in the radial direction $\mathrm{Pe} = RU_r/D_\mathrm{v} = \mathrm{O}(10^2)$ (R is the radius after droplet spreading, ~100 µm; U_r is the radial velocity of internal flow, $\mathrm{O}(10^{-4})$ m s^{-1}; D_v is the diffusion coefficient of the micelles, $\mathrm{O}(10^{-10})$ m^2 s^{-1} for spherical or ellipsoidal micelles), indicating that convection of micelles dominates over diffusion. Therefore, we expect the concentration of micelles close to the TCL to increase rapidly during evaporation due to the singularity in the evaporation flux at the TCL and the outward capillary flows. For an equilibrium $C_nE_m/\mathrm{H_2O}$ system at the ambient temperature of around 21 °C in our experiments, a phase transition from a micellar solution to a liquid crystalline mesophase occurs with increase of surfactant concentration, e.g., from around 40 wt.% for an equilibrium system of

$C_{12}E_8/H_2O$.[29] While there have been several studies on the evaporation of binary or ternary liquid mixtures that pass through a binodal as the more volatile component(s) evaporate[23, 37-38], phase transitions in sessile droplets of surfactant solutions triggered by evaporation have not been reported. One of the objectives of this study was to discover whether the existence of intermediate mesophases in C_nE_m solutions had a marked effect on drying dynamics compared to another surfactant, such as SDS, that transforms directly to a hydrated crystal upon drying at room temperature. Our experiments revealed distinctive drying characteristics of C_nE_m-laden droplets that we argue are related to phase transitions from a micellar solution to a mesophase during evaporation. The exact nature of the transient mesophase has not been established. The wetting dynamics and internal flows are also discussed in the paper.

MATERIALS AND METHODS

Materials. A homologous series of pure non-ionic surfactants polyoxyethylene glycol monoalkyl ethers (C_nE_m: $CH_3(CH_2)_{n-1}(OCH_2CH_2)_mOH$), including $C_{10}E_8$, $C_{12}E_8$, $C_{14}E_8$ and $C_{14}E_6$ were studied as well as the anionic surfactant SDS ($C_{10}E_8$ and $C_{12}E_8$, ≥ 98%, and SDS, > 99%, were purchased from Sigma-Aldrich and used as received; $C_{14}E_8$ and $C_{14}E_6$ were purchased from Nikko Chemicals Co. Ltd. and used as received). Table 1 lists some physicochemical properties of these surfactants, including CMC, surface tension at CMC, micelle shape and hydrophile–lipophile balance (HLB). The aqueous solutions were prepared using ultrapure water (Chorus 1 Analytical Research, Elga). A stock solution of 20 mM was prepared first; solutions with lower concentrations of surfactants were prepared by diluting the stock solutions. The concentrations of C_nE_m solutions were 0.5, 1, 5 and 10 mM. For SDS solutions, the concentrations were 5, 10 and 20 mM. For experiments on internal flows during the evaporation of a picoliter droplet, 0.04–0.05

vol % polystyrene (PS) particles were added as tracers (median diameter 997 nm, steric stabilized by polyethylene glycol methacrylate (PEGMA);[39] University of Leeds, U.K.).

The majority of the experiments were conducted with hydrophilic substrates (plasma-cleaned glass coverslips, Academy Science, 0.13–0.17 mm thickness, freshly cleaned on the day of experiments, fully wettable by water). Hydrophobic substrates (hexamethyldisilazane-modified glass coverslips, equilibrium water contact angle 72±2 °) were used in a few tests for a comparative study. The results presented in this paper are for droplets evaporating on hydrophilic substrates if not specified.

Table1. Summary of basic properties of surfactants (at 25 °C)[30, 40].

Surfactant	CMC (mM)	σ (mN m^{-1})	Micelle shape	HLB
$C_{10}E_8$	1	35.5	Spheroidal	13.0
$C_{12}E_8$	0.07	34.3	Spheroidal	11.9
$C_{14}E_8$	0.01	34	Spheroidal	11.0
$C_{14}E_6$	0.01	31	Rod/Wormlike	9.6
SDS	8.1	35	Spheroidal	40

Methods. Droplets (200 ± 50 pL) were ejected from a drop-on-demand inkjet print head (MJ-ABP-01, Microfab Technologies) with a 50 μm-diameter orifice onto a transparent glass substrate. The Weber number, We=$\rho U_i^2 D_s/\sigma$= O (1) (ρ is the liquid density, ~10^3 kg m^{-3} ; U_i is the impact velocity, ~ 1 m s^{-1}; D_s is the diameter of the spherical droplet before landing, ~70 μm; σ is the liquid surface tension), is O (1) and spreading is driven by capillary forces within 1 ms after impact. The printing experiments were conducted in ambient environment with temperature T = 21 ± 0.5 °C and relative humidity RH = 40% ± 10%. A custom-made optical apparatus (see Figure S1) was used to observe and record the drying process of a droplet. A schematic of the printing rig can be found in Figure S1 and a detailed description of the experimental apparatus can be found elsewhere.[41]

We first carried out morphological studies. Surfactant solutions were printed on a substrate and the spreading and retracting of a droplet were recorded simultaneously from the side and from below with two high-speed cameras. Interference fringes are visible from the bottom view when local heights of a liquid film are within half the coherence length (ca. 5.5 μm), where a blue LED light and a bandpass filter were used to control the coherence length. Successive bright (or dark) fringes are separated in thickness by 177 nm in water. The three-phase contact line of a drying droplet from the bottom view was tracked by custom-written Matlab codes and the contact diameter was extracted as a function of elapsed time *t*. The thickness and contact angle of a drying droplet with time were extracted from interference images (refer to Figure S2 for illustration of the image analysis process). The shadow image of a drying droplet from the side view was tracked when the contact angle is above 5° and parameters of interest such as the contact diameter and contact angle were extracted as a function of *t*.

Second, we studied internal flows of droplets during the drying process. Surfactant solutions with tracer particles were printed on a substrate with oblique illumination; the scattered light from the tracer particles is visible from the bottom view as a dark-field image. Trajectories of the tracer particles were derived using particle-tracking code adapted from open source software developed at Georgetown University.[42]

RESULTS AND DISCUSSION

General picture of the drying process. Figure 1 shows a typical sequence of bottom-view images for pure water droplets and SDS-laden droplets on hydrophilic glass substrates. A water droplet relaxes and spreads upon landing on the substrate followed by retraction due to evaporation of water (Figure 1(a)). 5 mM SDS droplets show qualitatively similar drying behaviour to pure water except that the receding contact angle is higher (which can be seen from the closer spacing of the interference fringes) and that "foot-prints" of dried SDS are left behind the receding droplet (Figure 1(b) and Movie S1).

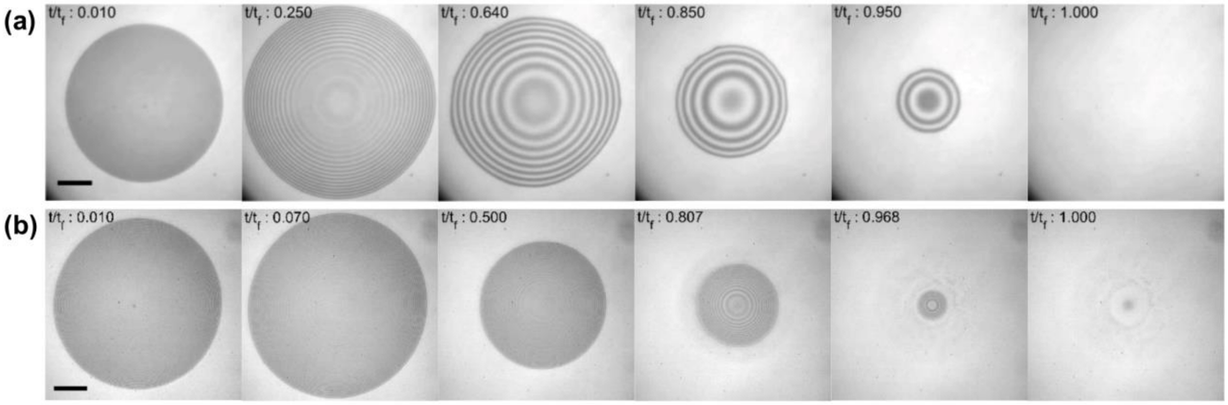

Figure 1. Bottom-view images during the drying of a pure water droplet (a, $t_f = 0.98$ s) and a 5 mM SDS droplet (b, $t_f = 1.28$ s). Scale bars for 50 µm and t_f denotes the vanishing time of a receding droplet.

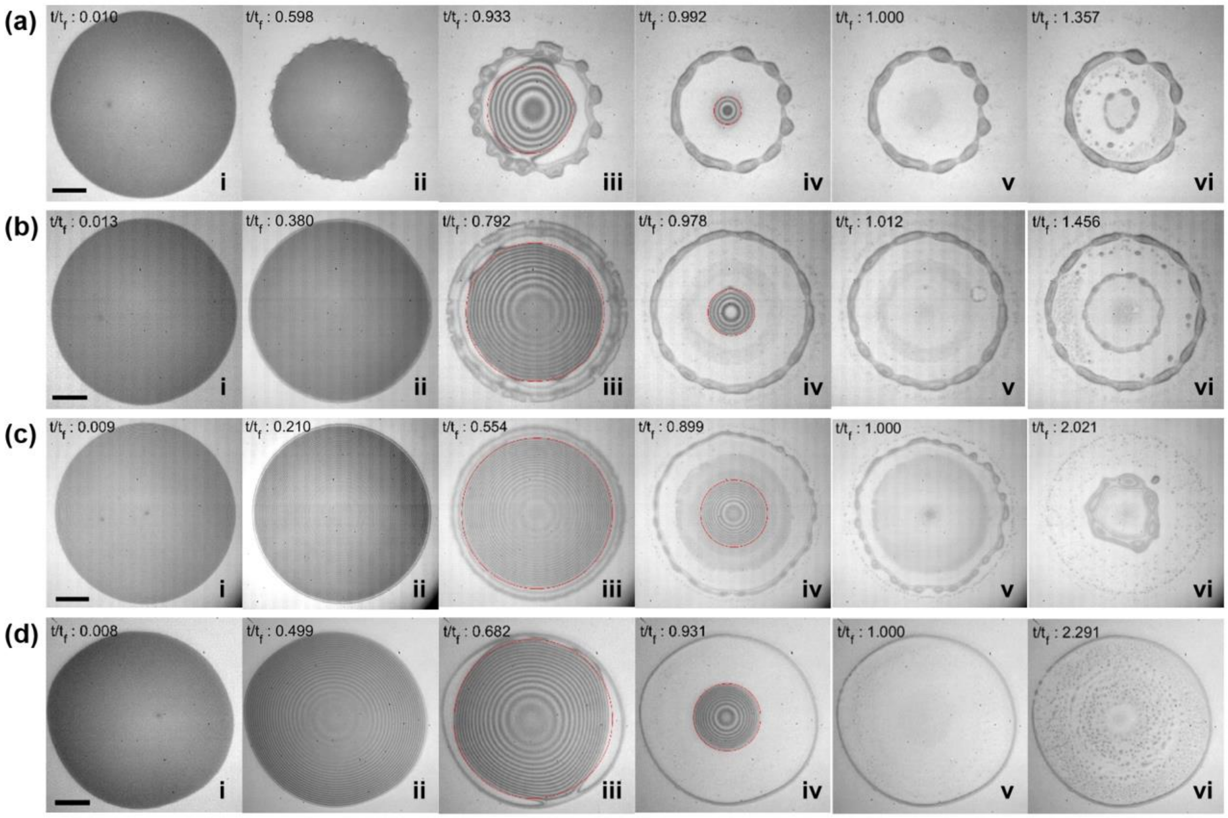

Figure 2. Bottom-view images during the drying of C_nE_m droplets. Scale bars are 50 μm. t_f denotes the vanishing time of a receding water-rich droplet and the red lines illustrate tracked contact lines of the receding droplets. (a) 5 mM $C_{10}E_8$, t_f = 1.71 s; (b) 5 mM $C_{12}E_8$, t_f = 1.47 s; (c) 5 mM $C_{14}E_8$, t_f = 1.43 s; (d) 5 mM $C_{14}E_6$, t_f = 1.08 s.

In contrast to the simple drying behaviour of SDS droplets, C_nE_m droplets show complex drying dynamics, as shown in Figure 2 (refer to corresponding movies S2–S5 in SI). Though each surfactant shows subtly different drying characteristics, a consistent feature stands out — a droplet that contains the major liquid volume fraction retracts continuously until it vanishes while leaving a thin film behind. The main droplet behaves like a water-rich phase: it dries in 1–2 s, which is comparable to the drying time of a pure water droplet of the same initial volume. We label the drying time of the central droplet, t_f. The thin film typically breaks up into a myriad of small droplets 1–2 s after the vanishing of the main droplet, sometimes leaving a ring or central puddle, which take minutes to dry out. The persistence of the fluid in the thin film indicates that it is a water-poor / surfactant-rich phase.

The drying characteristics suggest that the C_nE_m droplets undergo a phase separation during the drying process. A close examination of the drying process reveals that a film starts to appear at the periphery of the droplet, usually after initial spreading (Figure 2(bii–dii) but occasionally after the contact line had already retracted some distance (Figure 2(aii)), and grows to a thickness of $O(10^2)$ nm. The annular rim pins the liquid–solid contact line and increases in width until at some point the water-rich droplet detaches from the rim (Figure 2(aiii–diii)). The central water-rich cap then retracts leaving behind a much thinner film (Figure 2(aiv–div)). The rim either remains pinned or retracts slowly and develops festoon-like waves, possibly due to a Rayleigh-Plateau instability. The water-rich droplet evaporates completely leaving a very thin (< 100 nm) film covering the whole of the contact area confined by the annular rim. The contrast within this film (Figure 2(av–dv)) indicates the presence of rings with variations in optical thickness (most likely due to actual thickness variations (darker regions are thicker) but possibly also due to differences in surfactant concentration). The thickness of the thin film appears to be related, inter alia, to the speed of the receding contact line between the water-rich cap and the thin film (see Figure S3). The fast contact line retraction after the water-rich cap detaches from the rim results in a thinner film near the outer rim. The thin film is unstable and either breaks into tiny droplets (e.g. Figure 2dvi, Movie S5) or breaks and shrinks inwards forming a thicker film with a smaller radius (Figure 2(avi–cvi)). The thin film tends to break up first in the thinner region near the outer rim. In some cases a second rim then develops which in turn exhibits an instability leading to a second festoon-like wave (Figure 2(avi, bvi), Movies S2, S3). Droplets with different concentrations of C_nE_m show qualitatively similar behaviour with some unsurprising differences: for example, the thin film left behind the retracting water-rich cap is thicker for higher surfactant concentrations (see Figure S4).

We attribute the behaviour observed in the drying of C_nE_m-laden droplets to phase transition(s) of the surfactant solution. Equilibrium phase diagrams of $C_{12}E_8/H_2O$ and SDS/H_2O systems available in the literature[29, 43] (Figure S5) detail the phase transitions that occur with increasing surfactant concentrations. For $C_{12}E_8$ solutions, the micelles form a hexagonal mesophase at a concentration around 38 wt% at 21 °C. As the surfactant concentration increases further, mesophase/mesophase transitions occur, from hexagonal to bicontinous cubic to lamellar. At the highest surfactant concentrations, the mesophase transforms to a reverse micellar solution and eventually to solid aggregates. For SDS solutions in equilibrium at around 21 °C, the micellar solution transforms directly to hydrated crystals at a concentration around 30 wt%; no mesophases are formed with increasing surfactant concentrations. We postulate that C_nE_m droplets undergo a phase transition from the micellar phase to a mesophase at the contact line where the surfactant concentration is highest. As the water-rich phase recedes it leaves behind a thin film of the mesophase. A rough calculation for a 5 mM $C_{14}E_8$-laden droplet at the vanishing of the water-rich droplet ($t/t_f = 1$), as shown in Figure 2c(v), with an approximate height of 90 nm (i.e., the height of the first dark fringe) in the central region and 360 nm in the rim, gives us an estimated film volume of about 1 pL and mean surfactant concentration of 50–60 wt% in the film. This concentration would correspond to a hexagonal mesophase in a $C_{14}E_8/H_2O$ system at equilibrium. (We note that the rapidly drying thin film may not follow the equilibrium phase diagram and the interactions with the surface could favour particular phases. The surfactant concentration is unlikely to be uniform as the mesophase continues to lose water by evaporation after it is formed.)

Subtle variations in the drying behaviour for different C_nE_m-laden droplets could be related to differences in the phase boundaries and rheology of different mesophases.

We propose the following general picture of the drying process of aqueous C_nE_m droplets, as shown in Figure 3. Upon landing on the glass substrate, the droplet quickly relaxes ($t < 1$ ms) and then spreads on the solid surface under capillary action. As the water in the droplet evaporates, the surfactant concentration close to the TCL increases rapidly (Figure 3(b)) – primarily because the droplet is thinnest here, augmented by the enhanced evaporation near the contact line and the transport of surfactant micelles to the periphery of the droplet by outward capillary flows. The high Peclet number of micelles ($O(10^2)$) limits the redistribution of the micelles in the radial direction. As the mass fraction of surfactant in the periphery of the droplet increases, the isotropic micellar solution undergoes a phase transition to an ordered mesophase, leading to an annular rim of the mesophase with slowly increasing width (Figure 3(c)). Hexagonal lyotropic mesophases, in particular, are highly viscous and will tend to pin the contact line. The water-rich droplet initially remains pinned but as the contact angle decreases it suddenly detaches from the mesophase and retracts rapidly. The water-rich phase is still evaporating as it retracts and so a thin film of the mesophase is deposited in the vicinity of the contact line of the receding water-rich droplet (Figure 3(d)); thus the area of the thin mesophase film continues to grow until the water-rich droplet dries completely (Figure 3(e)). The surfactant mesophase has a non-zero receding contact angle on the glass substrate and is not stable: it shrinks inwards and/or breaks into tiny droplets, eventually leaving a final surfactant deposit (Figure 3(f)).

We pose the question of whether the mesophase forms only at the contact line or at the solid–liquid interface beneath the water-rich cap. The Peclet number for transport of micelles in the vertical direction is ~ 0.2, based on an evaporation rate of 5 μm s^{-1} and a height, h, of 5 μm. A value of Pe < 1 but not << 1 indicates that diffusion is more important than convection, but that there will still be surfactant concentration gradients in the vertical direction with the concentration being highest at the free surface and lowest at the solid–liquid interface (in the absence of Marangoni-driven recirculation). Nonionic surfactants form bilayers on silica at concentrations just below the CMC[31] but we are not aware of any literature evidence that the bulk mesophase pre-wets the silica-water interface. Consequently, the mesophase would form at the air–liquid interface before it forms at the solid–liquid interface. We note also that the rim forms when the average concentration of surfactant in the droplet is still very much lower than its value at the phase boundary.

To provide supporting evidence for this drying model and additional insights into the drying process we have carried out a more detailed examination of the dynamics of drying of the surfactant-laden sessile droplets, specifically on spreading and retracting of the TCL, and on internal flows.

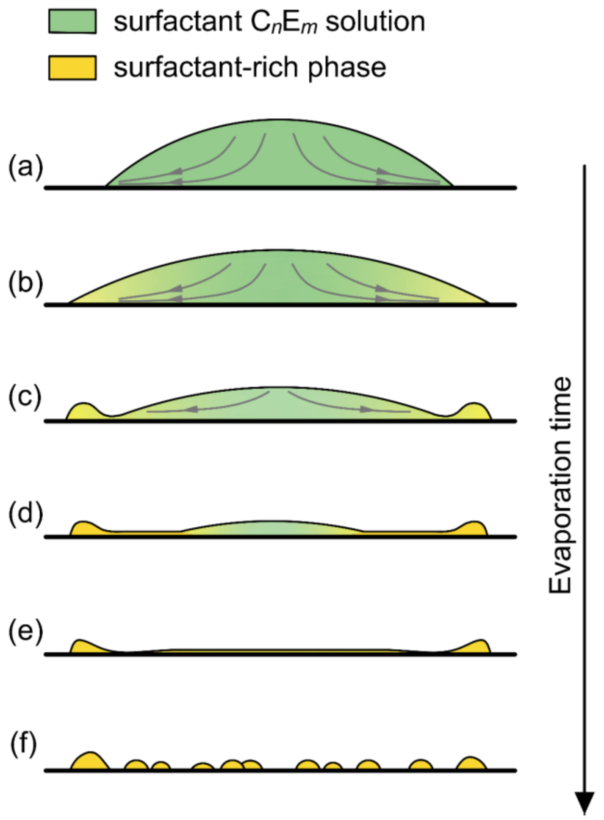

Figure 3. Illustration of the drying process of C_nE_m dissolved droplets. The scale in the sketches do not reflect real scales.

Spreading and retracting of droplets of aqueous surfactant solutions. Figure 4 plots the diameter of the contact line as a function of time for various concentrations of surfactant on hydrophilic substrates; pure water is shown for comparison. The diameter D is normalised by the diameter of the droplet immediately after the impact phase of the droplet (D_0) and the time t is normalised by the vanishing time of the retracting water-rich phase (t_f). The dimensionless drying curves of SDS-laden droplets are unified for different concentrations. Both SDS and pure water droplet retract immediately after spreading stops; the contact line does not pin. SDS inhibits spreading with outward motion ceasing at ~ $0.05t_f$, earlier compared to ~ $0.2t_f$ for pure water, giving a smaller maximum wetting diameter (Figure 4a). C_nE_m droplets were even more effective at suppressing spreading, with spreading ceasing as early as $t = \mathrm{O}(10^{-3})\ t_f$ (Figures 4(b-d)). At first sight it is unexpected that SDS and $\mathrm{C}_n\mathrm{E}_m$ solutions inhibit spreading on hydrophilic surfaces since surfactant solutions have lower surface tensions and hence higher spreading coefficients, *S,* than pure water ($S = \sigma_{sg} - \sigma_{sl} - \sigma_{lg},$ with σ denoting the interfacial tension, and subscripts *s*, *l*, and *g* denoting substrate, liquid and gas[44]). A probable mechanism behind the suppressed spreading is Marangoni contraction due to the radial surface tension gradient along the liquid–air interface. Marangoni stresses can either enhance or suppress spreading, depending on the direction of the surface tension gradients across the gas–liquid interface.[45-50] For surfactant solutions, the surface tension decreases strongly with concentration below the CMC and much more weakly above the CMC. The high radial Pe numbers lead to concentration gradients and hence a lower surface tension near the contact line than at the apex of the droplet. We observed inward surface flows in both SDS- and $\mathrm{C}_n\mathrm{E}_m$-laden droplets (presented in the next section). The only solution studied that is below the CMC (0.5 mM $\mathrm{C}_{10}\mathrm{E}_8$) showed the greatest inhibition of spreading, supporting a Marangoni mechanism. In addition, the proposed phase transition from a low-viscosity micellar solution to a viscous mesophase at the TCL is likely to play a role in suppressing spreading of $\mathrm{C}_n\mathrm{E}_m$ droplets. The mesophase pins the droplets and stops further spreading. Generally, for solutions above the CMC, droplets with higher concentrations of $\mathrm{C}_n\mathrm{E}_m$ pinned earlier. Unlike SDS, the $\mathrm{C}_n\mathrm{E}_m$ droplets remained pinned for a significant fraction of the drying time before retraction started.

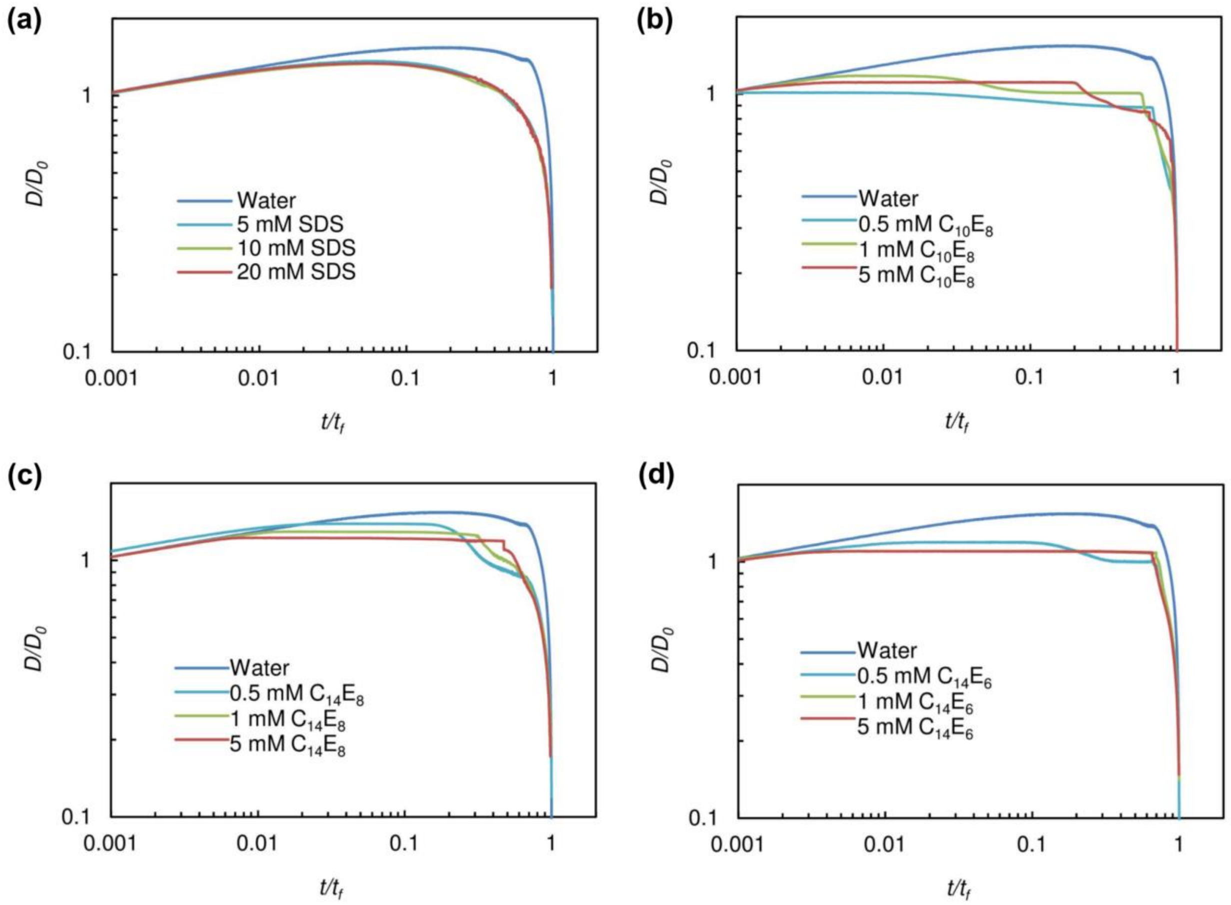

Figure 4. Dimensionless contact diameter versus dimensionless drying time for droplets with different surfactants. D is the diameter of the water (or water-rich) droplet, D_0 the diameter of the droplet upon landing and t_f the vanishing time of the water-rich droplet, t_f ~ 1 s. (a) SDS; (b) $C_{10}E_8$; (c) $C_{14}E_8$; (d) $C_{14}E_6$.

We can reconstruct the height profiles of droplets from the interference fringes in the bottom-view images (Figure 5). The droplets are generally well-fitted by spherical caps until the very late stage of evaporation. Evolution of contact angles calculated from the height profiles as well as evolution of the corresponding contact diameters is displayed in Figure 6. SDS-laden droplets retract normally as expected for a simple solution, with a receding contact angle, θ_r, that is approximately constant at 5–6° (Figure 6(b)) – a significantly higher value than that of pure water

(Figure 6(a)). By contrast, a “pinning-depinning jump” is observed in C_nE_m droplets (Figure 6(c) and (d)). For the $C_{14}E_m$ data shown, the contact line pins at early times ($t/t_f < 0.1$); D remains constant while both θ_r and h decrease as water evaporates. At a time between 0.3 and 0.8 t/t_f, depending on the surfactant and the concentration, the water-rich droplet depins from the annular rim. Its contact line retracts rapidly (Figure S3) and θ_r (Figure 6) and h (Figure 5) both increase for a short period. The rapid retraction of the contact line leads to a very thin film of the mesophase (Figure 2). When the contact angle reaches the value of the dynamic receding contact angle for the water-rich phase on top of the mesophase, the retraction speed and contact angle become approximately constant, with $\theta_r \sim$ 5–6°.

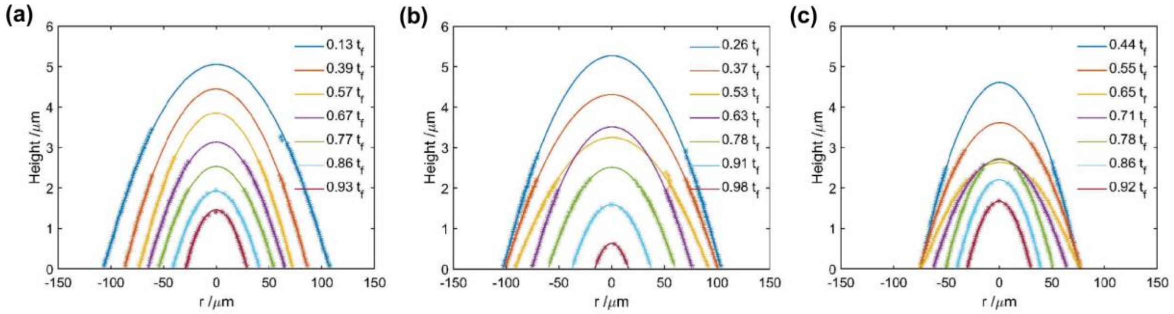

Figure 5. Evolution of height profiles of drying surfactant-laden droplets. The data points are extracted from interference fringes and the lines are spherical caps from curve fitting. t_f denotes the vanishing time of the receding droplet, $t_f \sim 1$ s. (a) 5 mM SDS; (b) 5 mM $C_{14}E_8$; (c) 5 mM $C_{14}E_6$. Note that after phase separation begins these figures show the profile of the water-rich phase and not the annular rim of the mesophase.

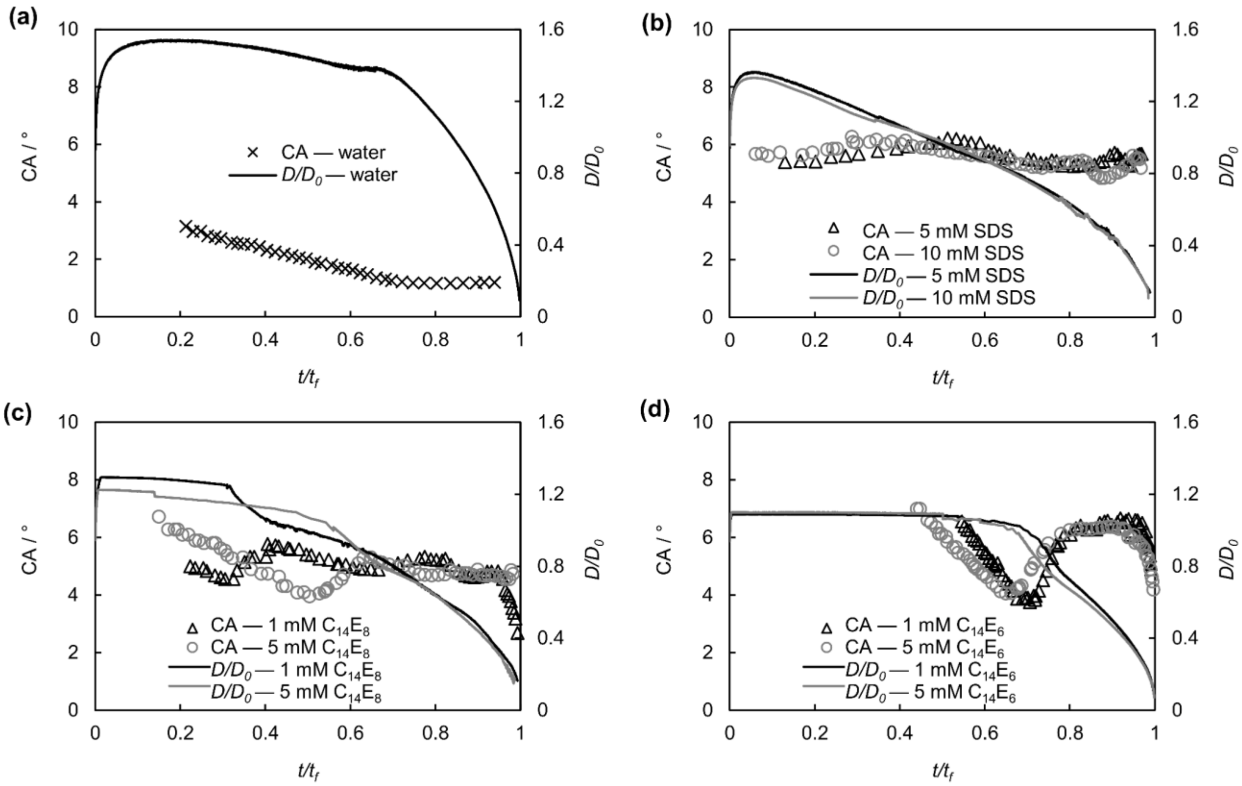

Figure 6. Evolution of the contact angle and contact diameter of a drying water droplet (a) and surfactant-laden (b-d, b: SDS; c: $C_{14}E_8$, d: $C_{14}E_6$) droplets on a hydrophilic substrate. t_f denotes the vanishing time of the receding droplet of the water-rich phase, $t_f \sim 1$ s. For $C_{14}E_6$ (d), the contact angle is too high at earlier times to yield distinct fringes from which the contact angle can be calculated reliably.

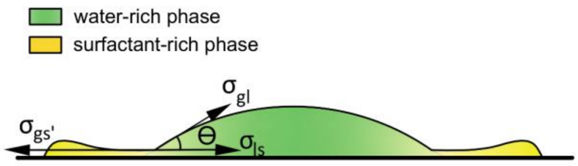

Figure 7. Illustration of forces at the three-phase contact line of a retracting water-rich droplet during the drying a C_nE_m-laden droplet.

The forces that act at the contact line of the retracting water-rich phase during the drying of a C_nE_m-laden droplet are depicted in Figure 7. The three surface tensions acting at the contact line are gas–substrate ($\sigma_{gs'}$), gas–liquid (σ_{gl}), and liquid–substrate (σ_{ls}) where we use subscripts s and s' to denote the substrate that is in close vicinity of the contact line, inside and outside the contact line respectively. Outside the contact line, the substrate is chemically modified by the mesophase. At air–liquid interfaces, surfactants orient themselves to expose the hydrophobic tails to air, generating a lower energy surface than clean glass. Underneath the droplet, a bilayer of surfactant exists,[31] with the hydrophilic poly(ethylene oxide) chains of the surfactants in contact with the aqueous phase. At equilibrium, the contact angle is determined by Young's equation ($\cos\theta_{eq} = \frac{\sigma_{gs'}-\sigma_{ls}}{\sigma_{gl}}$). It is reasonable to expect that $\sigma_{gs'} \cong \sigma_{gl}$, so $\cos\theta_{eq} \cong 1-\frac{\sigma_{ls}}{\sigma_{gl}}$ and hence $\theta_{eq} > 0$, implying that there is a thermodynamic driving force for the water-rich phase to dewet from a mesophase of the same surfactant. The dynamic receding contact angle (θ_r) is less than the equilibrium value due to dissipation of energy at the moving contact line. Viscous dissipation (expressed in the same dimensions as σ) scales as $\eta v/\theta_r$,[51] where v is the speed of the receding contact line and η the viscosity. Higher contact line speeds are associated with lower contact angles (i.e., higher inward force), which is what we observe experimentally (compare Figure 6(d) and Figure S3). A quantitative discussion on the dewetting dynamics, provided in the SI, shows that the receding contact angle and velocity of retraction of the contact line can be explained by a simple model that balances the capillary force with viscous dissipation in a droplet with a viscosity close to that of pure water. Since the surface energy of the substrate with a thin film of surfactant mesophase phase, $\sigma_{gs'}$, is lower than that of the clean glass substrate (which must be greater than that of pure water (72 mN m^{-1}) since clean glass is wet by water), θ_r for C_nE_m solutions is higher than that for pure water. θ_r for SDS solutions is similar to that of C_nE_m solutions despite the fact that the physical chemistry of two systems is quite different: anionic SDS does not adsorb at negatively charged glass-water interfaces and it does not form a mesophase. It is plausible that the SDS deposits left on the surface by the receding droplet have a similar surface energy to the C_nE_m mesophases and that σ_{ls} is similar for both surfactants (C_nE_m bilayers only form on silica at concentrations very close to the CMC so the driving force for adsorption is weak), but it could also be that the similarity in θ_r is coincidental.

To test the model in Figure 7, we also studied the spreading and retraction of $C_{14}E_6$-laden droplets on a hydrophobic substrate. Nonionic surfactant solutions form monolayers on hydrophobic substrates, in contrast to the bilayers on hydrophilic substrates, but they expose their polar headgroups to the supernatant solution in either case.[32] In the latter stages of drying of $C_{14}E_6$ droplets on hydrophobic substrates, a water-rich phase detaches from the rim leaving behind a thin film that eventually breaks up into tiny droplets, similar to the case of hydrophilic substrates in Figure 2 (see Movie S6 in SI). If a surfactant mesosphase is formed as the water-rich droplet retracts, then we would expect θ_r to be similar on hydrophobic or hydrophilic surfaces despite the very different surface energies of the bare substrates.

The diameter and contact angle of $C_{14}E_6$ droplets during drying are shown in Figure 8. The contact angle was extracted both from side-view shadowgraph images (before $0.5t_f$ when $\theta > 5°$) and bottom-view interference images (after $0.9t_f$ when fringes become visible). The early-time dynamics are very different on hydrophobic and hydrophilic surfaces. On a hydrophobic surface, the surfactant enhances spreading compared to water. The contact line is pinned for the larger part of the drying time while the contact angle decreases from the advancing angle at the end of the spreading phase (10–20°) to the value at which the water-rich phase depins from the mesophase at the rim (2–3°). After depinning, θ_r increases to 5–6°, which is similar to the values on a hydrophilic surface as expected from our drying model.

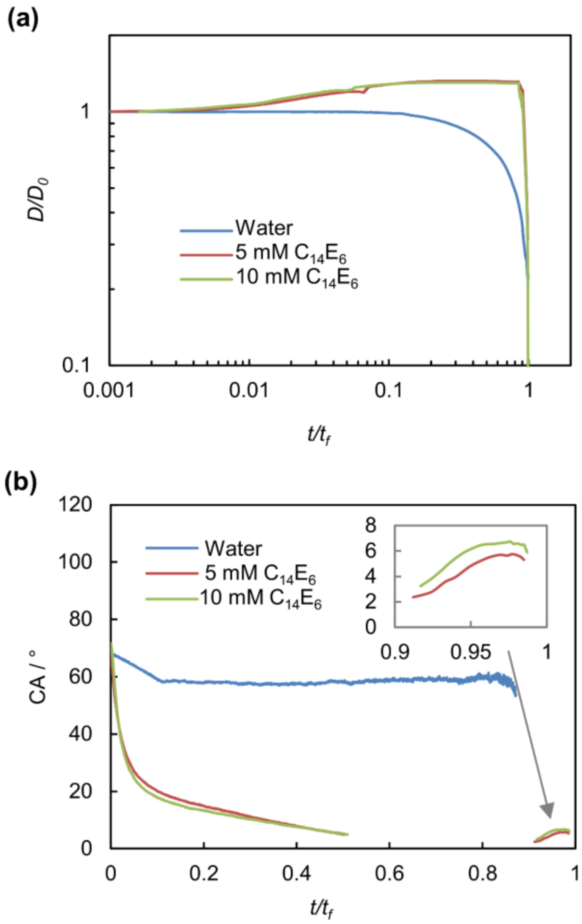

Figure 8. Spreading and retracting (a) and evolution of contact angle (b) of $C_{14}E_6$-laden droplets on a hydrophobic substrate. t_f denotes the vanishing time of the receding droplet, $t_f = 5.0$ s for the water droplet, and $t_f = 4.0$ s and 4.9 s for droplets with 5 mM and 10 mM $C_{14}E_6$, respectively.

An alternative explanation for our observations that should be considered is the effect of viscosity changes within a single phase. The effect of concentration-dependent viscosity together with Marangoni effect and interactions between particles and polymers have been reported to control the coffee-ring effect (CRE) in polymer solutions in Cui et al. (2012)[52]. The capillary number, Ca, in the drying droplets is $O(10^{-5})$ in our study ($Ca = \mu U_r/\sigma$, where μ the liquid viscosity, O (10^{-3} Pas), U_r is the radial velocity of internal flow, O (10^{-4} m s^{-1}), and σ is the liquid surface tension, O (10^{-2} N m^{-1})). Available evidence on the viscosity of C_nE_m solutions suggests that the isotropic L_1 (micellar phase) has a viscosity O(10 –10^2) higher than that of water at the L_1/mesophase boundary.[53] This viscosity increase is insufficient to lead to deviations from a spherical cap shape since Ca remains << 1. In a rapidly drying droplet, it is conceivable that liquid-crystalline mesophases do not nucleate and that the L_1 phase increases in concentration and viscosity to a point where Ca ~ 1 and deviations from a spherical cap shape are possible. However, a single phase with varying composition would have smoothly varying interfacial tensions and would not give rise to a well-defined contact angle between a spherical cap and a uniform thin film.

Internal flows during drying of surfactant dissolved droplets. Internal flows within droplets both modify the spreading dynamics and redistribute surfactant, affecting the deposition of material at the contact line. We used tracer particles to follow the internal flows in drying droplets of C_nE_m solutions, again with SDS as a comparator. We note that tracer particles only measure flows in regions of the droplet where the thickness of the droplet is greater than the particle diameter and that they modify the fluid dynamics near the TCL (notably by pinning it). The dominant internal flows observed during drying of surfactant solutions on hydrophilic substrates are summarised in Table S1. Trajectories of tracer particles and illustration of internal flows during the evaporation of C_nE_m droplets are shown in Figure 9. Outward capillary flows as shown in Figure 9 (a, A) are dominant for droplets with lower concentrations (0.5 and 1 mM in this study) of C_nE_m. Marangoni flows towards the apex of a droplet alongside outward capillary flows (distinguished by focusing near the substrate and near the droplet apex) were observed for droplets with higher concentrations (5 and 10 mM in this study) of C_nE_8 with n = 10, 12 and 14 (Figure 9(b, B)). The Marangoni flows are mild relative to those seen in binary liquid mixtures[54-56] with no evidence for recirculating eddies at the contact line. Tracer particles close to the free surface moved inwards at first (observed with the focus ~ 4 μm above the substrate, i.e., near the droplet apex) and outward later following capillary flows (observed with the focus at the substrate). Particles near the contact line were then swept up by the retracting TCL. No Marangoni flows were observed after ~0.6 t_f, which is close to the time when the water-rich droplet detaches from surrounding surfactant-rich phase. For droplets with higher concentrations of $C_{14}E_6$ (5 and 10 mM in this study), no definitive Marangoni flows were observed. Quick retraction of the TCL induced inward movements of particles close to the TCL; some inward movements of particles far from the TCL were also observed, which can be caused by the free surface retraction or Marangoni flows or a combination of both.

SDS solutions exhibited Marangoni flows for initial concentrations above and below the CMC (Figure 10). These flows were stronger with SDS than with C_nE_8 (see Figure S7 for the velocity map), but ceased earlier, at around 0.3 t_f. More discussion on the deposit morphology of colloidal surfactant solutions is presented in the SI.

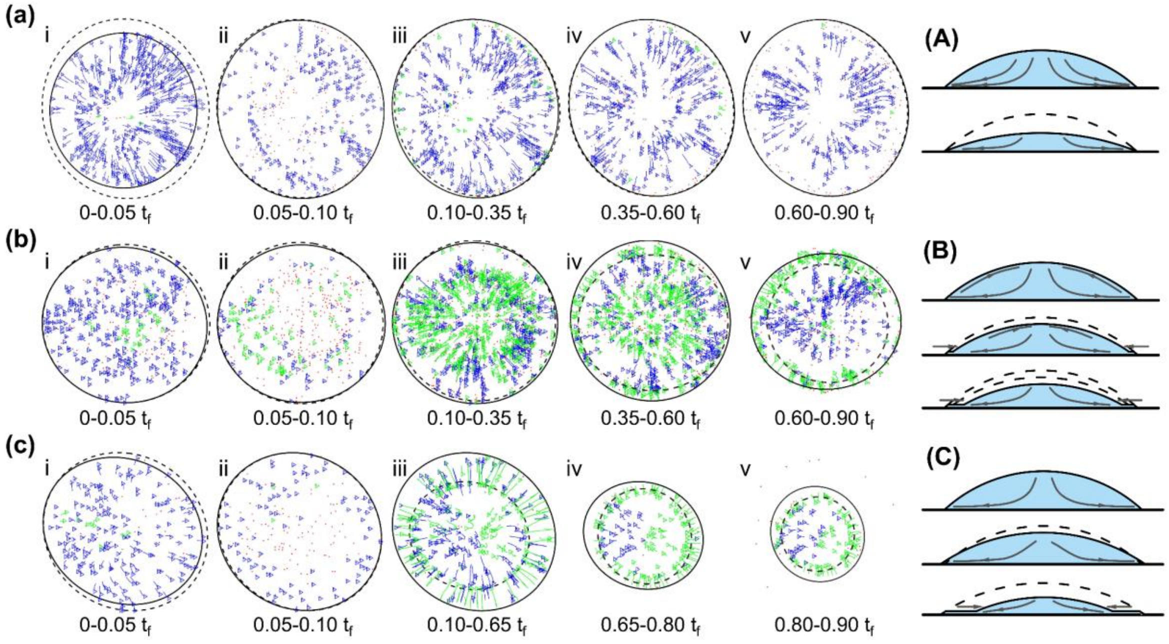

Figure 9. Trajectories of tracer particle (a, b, c) and sketches of internal flows (A, B, C) during the evaporation of C_nE_m droplets containing 0.05 vol % PS particles. (a, A) 0.5 mM $C_{14}E_8$; (b, B) 10 mM $C_{14}E_8$; (c, C) 10 mM $C_{14}E_6$. $\boldsymbol{t_f}$ denotes the vanishing time of the receding droplet, $t_f \sim 1$ s. For the trajectories, the red dots represent the stationary particles in the radial direction (movement < three pixels in the time interval), the blue and green lines represent outward and inward trajectories, respectively. The bold line and the dashed line represent the contact line at the start and end of the corresponding time-bin, respectively.

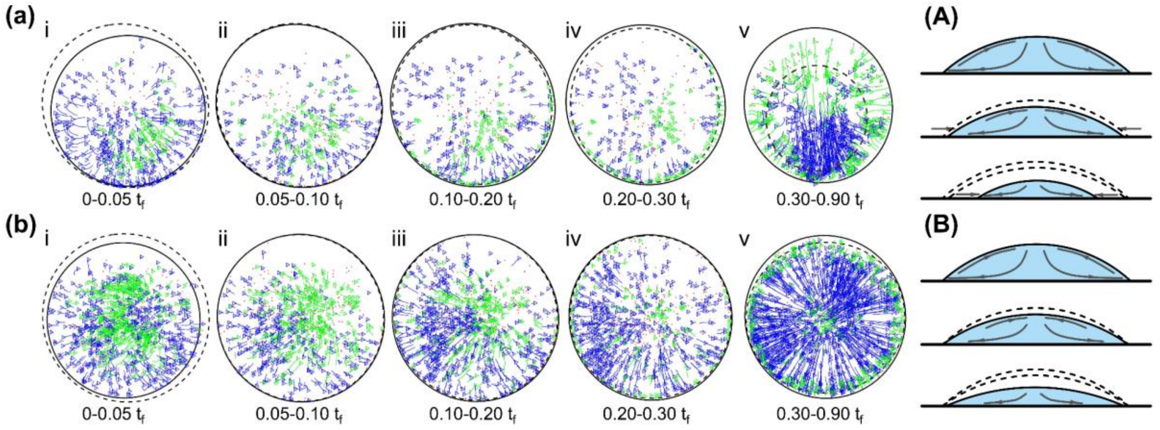

Figure 10. Trajectories of tracer particles (a, b) and sketches of internal flows (A, B) during the evaporation of SDS dissolved droplets containing 0.05 vol % PS particles. (a, A) 5 mM SDS, (b, B) 20 mM SDS. t_f denotes the vanishing time of the receding droplet, $t_f \sim 1$ s. For the trajectories, the red dots represent the stationary particles in the radial direction (movement < three pixels in the time interval), the blue and green lines represent outward and inward trajectories, respectively. The bold line and the dashed line represent the contact line at the start and end of the corresponding time-bin, respectively.

The observed Marangoni flow directed toward the apex of droplets serves as evidence of the existence of the Marangoni stresses that we hypothesised to contribute to the suppressed spreading of surfactant-laden droplets. Definitive Marangoni flows were not observed for droplets with lower concentrations of C_nE_m for which suppressed spreading was also demonstrated; it is likely that the Marangoni stresses are not sufficiently high to generate recirculating flows (with inward moving particles) but still oppose the capillary flows sufficiently to suppress spreading. We note that Marangoni stresses / Marangoni flows exist in the surfactant-laden droplets with concentrations both below and above the CMC. The Marangoni flows are stronger at higher concentrations of surfactants. Marangoni stresses / Marangoni flows are caused by a radial gradient in the dynamic surface tension. [57-60] The flow direction indicates that the dynamic surface tension at the apex of the droplet is higher than that at the TCL.

The existence of Marangoni flows at surfactant concentrations above the CMC is unexpected, since to a first approximation the surface tension is independent of surfactant concentration above the CMC; therefore gradients in surfactant concentration due to evaporation do not lead to surface tension gradients that drive Marangoni flows. There are two possible explanations for the observed behavior. The first is that, while the slope of a surface tension versus log concentration plot typically changes by about two orders of magnitude at the CMC, the surface tension does still decrease slowly with increasing surfactant concentration above the CMC due to interactions between micelles (the same interactions that ultimately lead to phase transitions). Marangoni flows are observed[50] in binary liquid mixtures with differences in surface tension of ~1 mN m^{-1} and such a difference in surface tension is plausible over the range of concentration from the CMC to the mesophase transition in C_nE_m surfactants. The second is that the dynamic surface tension in drying droplets differs from the equilibrium surface tension due to slow surfactant kinetics, either of desorption of surfactant from evaporating surface or the formation of micelles from monomeric surfactant. Either of these processes would lead to an increase in the dynamic surface excess above the equilibrium value and a lowering of the surface tension.

CONCLUSIONS

The drying of picoliter droplets containing aqueous solutions of non-ionic surfactants C_nE_m has been studied systematically and compared with behaviour of SDS solutions. C_nE_m droplets show qualitatively different behaviour which we hypothesise is due to a surfactant phase transition in C_nE_m solutions. The non-ionic surfactant solutions undergo phase separation at the contact line, where evaporation is fastest, into a water-rich phase and a rim of a surfactant mesophase. The water-rich phase detaches from the rim and retracts as a spherical cap with an approximately constant contact angle leaving behind a thin film of the surfactant mesophase. On a longer timescale, the thin film retracts and/or breaks up into tiny droplets. By contrast, a drying SDS-laden droplet simply leaves “foot-prints” of dried SDS as it retracts immediately after spreading. The existence of the mesophase film is corroborated by tests conducted on hydrophobic substrates which showed that the receding contact angle at the late stage of a drying C_nE_m-laden droplet is independent of the hydrophobicity of the substrate, as formation of mesophase film chemically modifies the substrate. The drying dynamics influences the deposition of colloidal particles suspended in the surfactant solutions and is therefore important in determining the morphology of the deposit, with consequential impact on the performance of devices manufactured by inkjet printing.

This study also showed that surfactant solutions do not necessarily enhance spreading compared to water. Both C_nE_m and SDS solutions inhibit spreading on hydrophilic surfaces; we attribute this phenomenon to Marangoni contraction due to a surface tension gradient across the gas–liquid interface. In addition, the phase transition at the initial TCL contributes to the more pronounced suppression of droplet spreading for C_nE_m solutions. Particle tracking reveals Marangoni flows directed towards the apex of the droplets at surfactant concentrations well above CMC, showing that even in micellar solutions surface tension gradients can cause Marangoni effects large enough to influence wetting dynamics.

ASSOCIATED CONTENT

Supporting Information

The following files are available free of charge via the Internet at http://pubs.acs.org.

Additional figures and discussions (PDF).

Movie S1 (AVI) – the drying process for a droplet with 5 mM SDS on a hydrophilic substrate; playback rate 0.1xReal time.

Movie S2 (AVI) – the drying process for a droplet with 5 mM $C_{10}E_8$ on a hydrophilic substrate; playback rate 0.1xReal time.

Movie S3 (AVI) – the drying process for a droplet with 5 mM $C_{12}E_8$ on a hydrophilic substrate; playback rate 0.1xReal time.

Movie S4 (AVI) – the drying process for a droplet with 5 mM $C_{14}E_8$ on a hydrophilic substrate; playback rate 0.1xReal time.

Movie S5 (AVI) – the drying process for a droplet with 5 mM $C_{14}E_6$ on a hydrophilic substrate; playback rate 0.1xReal time.

Movie S6 (AVI) – the drying process for a droplet with 10 mM $C_{14}E_6$ on a hydrophobic substrate; playback rate 1xReal time.

Movie S7 (AVI) – internal flows (shown by added tracer particles) during the drying process of a droplet with 0.5 mM $C_{14}E_8$ on a hydrophilic substrate; playback rate 0.05xReal time.

Movie S8 (AVI) – internal flows (shown by added tracer particles) during the drying process of a droplet with 10 mM $C_{14}E_8$ on a hydrophilic substrate; playback rate 0.05xReal time.

Movie S9 (AVI) – internal flows (shown by added tracer particles) during the drying process of a droplet with 10 mM $C_{14}E_6$ on a hydrophilic substrate; playback rate 0.05xReal time.

Movie S10 (AVI) – internal flows (shown by added tracer particles) during the drying process of a droplet with 5 mM SDS on a hydrophilic substrate; playback rate 0.05xReal time.

Movie S11 (AVI) – internal flows (shown by added tracer particles) during the drying process of a droplet with 20 mM SDS on a hydrophilic substrate; playback rate 0.05xReal time.

AUTHOR INFORMATION

Corresponding Author

*E-mail: c.d.bain@durham.ac.uk

Notes

The authors declare no competing financial interest.

ACKNOWLEDGMENT

This work was funded by EPSRC under Grant EP/N025245/1.

REFERENCES

1. Hanyak, M.; Darhuber, A. A.; Ren, M., Surfactant-induced delay of leveling of inkjet-printed patterns. *Journal of Applied Physics* **2011,** *109* (7), 074905.
2. Yoon, B.; Ham, D. Y.; Yarimaga, O.; An, H.; Lee, C. W.; Kim, J. M., Inkjet printing of conjugated polymer precursors on paper substrates for colorimetric sensing and flexible electrothermochromic display. *Advanced Materials* **2011,** *23* (46), 5492-5497.
3. Sun, J.; Bao, B.; He, M.; Zhou, H.; Song, Y., Recent advances in controlling the depositing morphologies of inkjet droplets. *ACS applied materials & interfaces* **2015,** *7* (51), 28086-28099.
4. Wang, Y.; Deng, R.; Yang, L.; Bain, C. D., Fabrication of monolayers of uniform polymeric particles by inkjet printing of monodisperse emulsions produced by microfluidics. *Lab on a Chip* **2019,** *19* (18), 3077-3085.
5. Deng, R.; Wang, Y.; Yang, L.; Bain, C. D., In Situ Fabrication of Polymeric Microcapsules by Ink-Jet Printing of Emulsions. *ACS applied materials & interfaces* **2019,** *11* (43), 40652-40661.
6. Pu, N.-W.; Wang, C.-A.; Liu, Y.-M.; Sung, Y.; Wang, D.-S.; Ger, M.-D., Dispersion of graphene in aqueous solutions with different types of surfactants and the production of graphene films by spray or drop coating. *Journal of the Taiwan Institute of Chemical Engineers* **2012,** *43* (1), 140-146.
7. Song, M.; Ju, J.; Luo, S.; Han, Y.; Dong, Z.; Wang, Y.; Gu, Z.; Zhang, L.; Hao, R.; Jiang, L., Controlling liquid splash on superhydrophobic surfaces by a vesicle surfactant. *Science advances* **2017,** *3* (3), e1602188.
8. Xu, L.; Zhu, H.; Ozkan, H. E.; Thistle, H. W., Evaporation rate and development of wetted area of water droplets with and without surfactant at different locations on waxy leaf surfaces. *biosystems engineering* **2010,** *106* (1), 58-67.
9. Lin, H.; Zhou, H.; Xu, L.; Zhu, H.; Huang, H., Effect of surfactant concentration on the spreading properties of pesticide droplets on Eucalyptus leaves. *Biosystems Engineering* **2016,** *143*, 42-49.

10. Damato, T. C.; Carrasco, L. D.; Carmona-Ribeiro, A. M.; Luiz, R. V.; Godoy, R.; Petri, D. F., The interactions between surfactants and the epicuticular wax on soybean or weed leaves: Maximal crop protection with minimal wax solubilization. *Crop protection* **2017,** *91*, 57-65.
11. Stoebe, T.; Lin, Z.; Hill, R. M.; Ward, M. D.; Davis, H. T., Surfactant-enhanced spreading. *Langmuir* **1996,** *12* (2), 337-344.
12. Karapetsas, G.; Craster, R. V.; Matar, O. K., On surfactant-enhanced spreading and superspreading of liquid drops on solid surfaces. *Journal of fluid mechanics* **2011,** *670*, 5-37.
13. Kovalchuk, N.; Trybala, A.; Arjmandi-Tash, O.; Starov, V., Surfactant-enhanced spreading: Experimental achievements and possible mechanisms. *Advances in colloid and interface science* **2016,** *233*, 155-160.
14. Deegan, R. D.; Bakajin, O.; Dupont, T. F.; Huber, G.; Nagel, S. R.; Witten, T. A., Capillary flow as the cause of ring stains from dried liquid drops. *Nature* **1997,** *389*, 827.
15. Hu, H.; Larson, R. G., Evaporation of a sessile droplet on a substrate. *The Journal of Physical Chemistry B* **2002,** *106* (6), 1334-1344.
16. Hu, H.; Larson, R. G., Analysis of the effects of Marangoni stresses on the microflow in an evaporating sessile droplet. *Langmuir* **2005,** *21* (9), 3972-3980.
17. Kajiya, T.; Kobayashi, W.; Okuzono, T.; Doi, M., Controlling the drying and film formation processes of polymer solution droplets with addition of small amount of surfactants. *The Journal of Physical Chemistry B* **2009,** *113* (47), 15460-15466.
18. Still, T.; Yunker, P. J.; Yodh, A. G., Surfactant-induced Marangoni eddies alter the coffee-rings of evaporating colloidal drops. *Langmuir* **2012,** *28* (11), 4984-4988.
19. Kim, H.; Boulogne, F.; Um, E.; Jacobi, I.; Button, E.; Stone, H. A., Controlled uniform coating from the interplay of Marangoni flows and surface-adsorbed macromolecules. *Physical review letters* **2016,** *116* (12), 124501.
20. Kwieciński, W.; Segers, T.; Van Der Werf, S.; Van Houselt, A.; Lohse, D.; Zandvliet, H. J.; Kooij, S., Evaporation of dilute sodium dodecyl sulfate droplets on a hydrophobic substrate. *Langmuir* **2019,** *35* (32), 10453-10460.
21. Yan, Q.; Gao, L.; Sharma, V.; Chiang, Y.-M.; Wong, C., Particle and substrate charge effects on colloidal self-assembly in a sessile drop. *Langmuir* **2008,** *24* (20), 11518-11522.
22. Anyfantakis, M.; Geng, Z.; Morel, M.; Rudiuk, S.; Baigl, D., Modulation of the coffee-ring effect in particle/surfactant mixtures: the importance of particle–interface interactions. *Langmuir* **2015,** *31* (14), 4113-4120.
23. Tan, H.; Diddens, C.; Lv, P.; Kuerten, J.; Zhang, X.; Lohse, D., Evaporation-triggered microdroplet nucleation and the four life phases of an evaporating Ouzo drop. *Proceedings of the National Academy of Sciences* **2016,** *113* (31), 8642-8647.
24. Li, Y.; Lv, P.; Diddens, C.; Tan, H.; Wijshoff, H.; Versluis, M.; Lohse, D., Evaporation-triggered segregation of sessile binary droplets. *Physical review letters* **2018,** *120* (22), 224501.
25. Deegan, R. D., Pattern formation in drying drops. *Physical review E* **2000,** *61* (1), 475.
26. Marin, A.; Liepelt, R.; Rossi, M.; Kähler, C. J., Surfactant-driven flow transitions in evaporating droplets. *Soft Matter* **2016,** *12* (5), 1593-1600.
27. Clunie, J.; Corkill, J.; Goodman, J.; Symons, P.; Tate, J., Thermodynamics of non-ionic surface-active agent+ water systems. *Transactions of the Faraday Society* **1967,** *63*, 2839-2845.
28. Clunie, J.; Goodman, J.; Symons, P., Phase equilibria of dodecylhexaoxyethylene glycol monoether in water. *Transactions of the Faraday Society* **1969,** *65*, 287-296.
29. Mitchell, D. J.; Tiddy, G. J.; Waring, L.; Bostock, T.; McDonald, M. P., Phase behaviour of polyoxyethylene surfactants with water. Mesophase structures and partial miscibility (cloud

points). *Journal of the Chemical Society, Faraday Transactions 1: Physical Chemistry in Condensed Phases* **1983,** *79* (4), 975-1000.
30. Schick, M. J., *Nonionic surfactants: physical chemistry*. CRC Press: New York, 1987.
31. Tiberg, F.; Joensson, B.; Tang, J.-a.; Lindman, B., Ellipsometry studies of the self-assembly of nonionic surfactants at the silica-water interface: equilibrium aspects. *Langmuir* **1994,** *10* (7), 2294-2300.
32. Tiberg, F., Physical characterization of non-ionic surfactant layers adsorbed at hydrophilic and hydrophobic solid surfaces by time-resolved ellipsometry. *Journal of the Chemical Society, Faraday Transactions* **1996,** *92* (4), 531-538.
33. Cachile, M.; Cazabat, A.; Bardon, S.; Valignat, M.; Vandenbrouck, F., Spontaneous spreading of surfactant solutions on hydrophilic surfaces. *Colloids and Surfaces A: Physicochemical and Engineering Aspects* **1999,** *159* (1), 47-56.
34. Ivanova, N. A.; Zhantenova, Z. B.; Starov, V., Wetting dynamics of polyoxyethylene alkyl ethers and trisiloxanes in respect of polyoxyethylene chains and properties of substrates. *Colloids and Surfaces A: Physicochemical and Engineering Aspects* **2012,** *413*, 307-313.
35. Lauger, J.; Linemann, R.; Richtering, W., Shear orientation of a lamellar lyotropic liquid crystal. *Rheologica acta* **1995,** *34* (2), 132-136.
36. Berni, M.; Lawrence, C.; Machin, D., A review of the rheology of the lamellar phase in surfactant systems. *Advances in colloid and interface science* **2002,** *98* (2), 217-243.
37. Li, Y.; Lv, P.; Diddens, C.; Tan, H.; Wijshoff, H.; Versluis, M.; Lohse, D., Evaporation-triggered segregation of sessile binary droplets. *arXiv preprint arXiv:1801.09885* **2018**.
38. Johns, A. Ink-Jet Printing of Multi-Phase Formulations. PhD Thesis, Durham University, 2017.
39. Yow, H. N.; Biggs, S., Probing the stability of sterically stabilized polystyrene particles by centrifugal sedimentation. *Soft Matter* **2013,** *9* (42), 10031-10041.
40. Berthod, A.; Tomer, S.; Dorsey, J. G., Polyoxyethylene alkyl ether nonionic surfactants: physicochemical properties and use for cholesterol determination in food. *Talanta* **2001,** *55* (1), 69-83.
41. Shi, J.; Yang, L.; Bain, C. D., Drying of ethanol/water droplets containing silica nanoparticles. *ACS applied materials & interfaces* **2019,** *11* (15), 14275-14285.
42. Blair, D.; Dufresne, E. The Matlab Particle Tracking Code Repository, http://site.physics.georgetown.edu/matlab/. [Accessed 1 May 2018].
43. Kekicheff, P.; Grabielle-Madelmont, C.; Ollivon, M., Phase diagram of sodium dodecyl sulfate-water system: 1. A calorimetric study. *Journal of colloid and interface science* **1989,** *131* (1), 112-132.
44. Probstein, R. F., *Physicochemical Hydrodynamics: An Introduction*. 2nd ed.; John Wiley & Sons: New York, 1994.
45. Pesach, D.; Marmur, A., Marangoni effects in the spreading of liquid mixtures on a solid. *Langmuir* **1987,** *3* (4), 519-524.
46. Ehrhard, P.; Davis, S. H., Non-isothermal spreading of liquid drops on horizontal plates. *Journal of Fluid Mechanics* **1991,** *229*, 365-388.
47. Ehrhard, P., Experiments on isothermal and non-isothermal spreading. *Journal of Fluid Mechanics* **1993,** *257*, 463-483.
48. Nikolov, A. D.; Wasan, D. T.; Chengara, A.; Koczo, K.; Policello, G. A.; Kolossvary, I., Superspreading driven by Marangoni flow. *Advances in colloid and interface science* **2002,** *96* (1-3), 325-338.

49. Karpitschka, S.; Liebig, F.; Riegler, H., Marangoni Contraction of Evaporating Sessile Droplets of Binary Mixtures. *Langmuir* **2017,** *33* (19), 4682-4687.
50. Hu, G.; Yang, L.; Yang, Z.; Wang, Y.; Jin, X.; Dai, J.; Wu, Q.; Liu, S.; Zhu, X.; Wang, X., A general ink formulation of 2D crystals for wafer-scale inkjet printing. *Science Advances* **2020,** *6* (33), eaba5029.
51. De Gennes, P.-G., Wetting: statics and dynamics. *Reviews of modern physics* **1985,** *57* (3), 827.
52. Cui, L.; Zhang, J.; Zhang, X.; Huang, L.; Wang, Z.; Li, Y.; Gao, H.; Zhu, S.; Wang, T.; Yang, B., Suppression of the coffee ring effect by hydrosoluble polymer additives. *ACS applied materials & interfaces* **2012,** *4* (5), 2775-2780.
53. Constantin, D.; Freyssingeas, É.; Palierne, J.-F.; Oswald, P., Structural transition in the isotropic phase of the C12EO6/H2O lyotropic mixture: a rheological investigation. *Langmuir* **2003,** *19* (7), 2554-2559.
54. Talbot, E.; Berson, A.; Yang, L.; Bain, C. In *Internal flows and particle transport inside picoliter droplets of binary solvent mixtures*, NIP & Digital Fabrication Conference, Society for Imaging Science and Technology: 2013; pp 307-312.
55. Talbot, E. Drying Inkjet Droplets-Internal Flows and Deposit Structure. PhD thesis, Durham University, 2014.
56. Talbot, E. L.; Yow, H. N.; Yang, L.; Berson, A. l.; Biggs, S. R.; Bain, C. D., Printing small dots from large drops. *ACS applied materials & interfaces* **2015,** *7* (6), 3782-3790.
57. Iliev, T. H.; Dushkin, C., Dynamic surface tension of micellar solutions studied by the maximum bubble pressure method. 1. Experiment. *Colloid and Polymer Science* **1992,** *270* (4), 370-376.
58. Eastoe, J.; Dalton, J. S.; Rogueda, P. G.; Crooks, E. R.; Pitt, A. R.; Simister, E. A., Dynamic surface tensions of nonionic surfactant solutions. *Journal of colloid and interface science* **1997,** *188* (2), 423-430.
59. Manglik, R. M.; Wasekar, V. M.; Zhang, J., Dynamic and equilibrium surface tension of aqueous surfactant and polymeric solutions. *Experimental thermal and fluid science* **2001,** *25* (1-2), 55-64.
60. Fainerman, V.; Mys, V.; Makievski, A.; Petkov, J.; Miller, R., Dynamic surface tension of micellar solutions in the millisecond and submillisecond time range. *Journal of colloid and interface science* **2006,** *302* (1), 40-46.

TOC Graphic

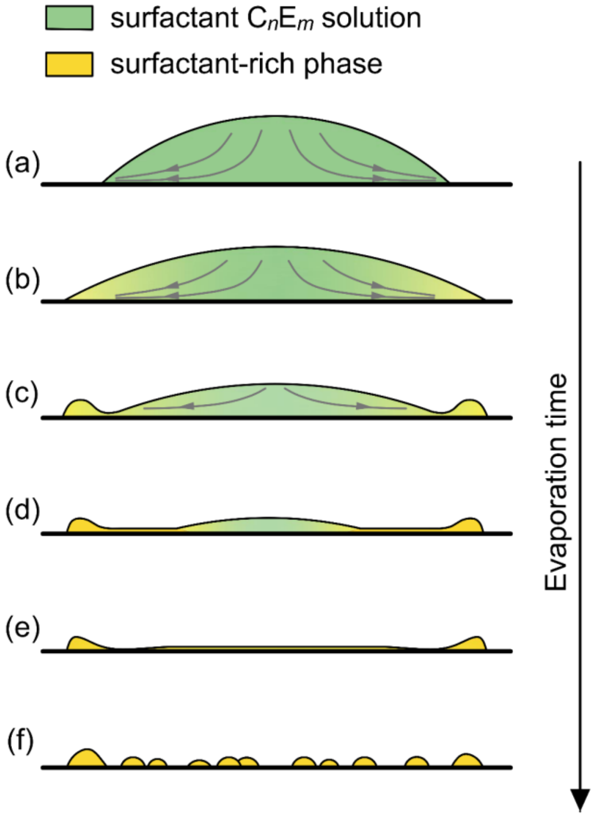

surfactant C_nE_m solution
surfactant-rich phase
(a)
(b)
(c)
(d)
(e)
(f)
Evaporation time